

Impact of predator dormancy on prey-predator dynamics

Joana G. Freire, Marcia R. Gallas, and Jason A. C. Gallas

Citation: *Chaos* **28**, 053118 (2018); doi: 10.1063/1.5016434

View online: <https://doi.org/10.1063/1.5016434>

View Table of Contents: <http://aip.scitation.org/toc/cha/28/5>

Published by the [American Institute of Physics](#)

PHYSICS TODAY

WHITEPAPERS

**ADVANCES IN PRECISION
MOTION CONTROL**

Piezo Flexure Mechanisms
and Air Bearings

READ NOW

PRESENTED BY

PI

Impact of predator dormancy on prey-predator dynamics

Joana G. Freire,^{1,2,a)} Marcia R. Gallas,^{1,2} and Jason A. C. Gallas^{1,2,b)}

¹*Instituto de Altos Estudos da Paraíba, Rua Silvino Lopes 419-2502, 58039-190 João Pessoa, Brazil*

²*Complexity Sciences Center, 9225 Collins Ave. Suite 1208, Surfside, Florida 33154, USA*

(Received 19 November 2017; accepted 4 May 2018; published online 24 May 2018)

The impact of predator dormancy on the population dynamics of phytoplankton-zooplankton in freshwater ecosystems is investigated using a simple model including dormancy, a strategy to avoid extinction. In addition to recently reported chaos-mediated mixed-mode oscillations, as the carrying capacity grows, we find surprisingly wide phases of nonchaos-mediated mixed-mode oscillations to be present well before the onset of chaos in the system. Nonchaos-mediated cascades display spike-adding sequences, while chaos-mediated cascades show spike-doubling. A host of braided periodic phases with exotic shapes is found embedded in a region of control parameters dominated by chaotic oscillations. We describe the organization of these complicated phases and show how they are interconnected and how their complexity unfolds as control parameters change. The novel nonchaos-mediated phases are found to be large and stable, even for low carrying capacity. *Published by AIP Publishing.* <https://doi.org/10.1063/1.5016434>

This paper reports a systematic investigation of the control parameter space of a model system incorporating effects of predator dormancy on the population dynamics of phytoplankton-zooplankton in freshwater ecosystems. Such a model was recently found to support chaos-mediated mixed-mode oscillations. In contrast, the present paper reports the discovery of surprisingly wide regular phases of nonchaos-mediated mixed-mode oscillations found to precede the onset of chaos in the system as the carrying capacity grows. Nonchaos-mediated cascades were observed only recently in distinct systems. They are characterized by spike-adding sequences of oscillations, while chaos-mediated cascades display the more common spike-doubling sequences of oscillations. Abundant periodic phases with exotic shapes are found embedded in a region of control parameters dominated by chaotic oscillations. The organization of all these complicated stability phases is described in detail. Furthermore, we show how phases of complex oscillations are interconnected and how their complexity unfolds as control parameters vary. Even at relatively low carrying capacity, nonchaos-mediated phases are found to be large and stable.

to destabilize the static coexistence of prey and predators in favor of stable periodic cycles. As the carrying capacity increases following the bifurcation, the amplitude of the periodic orbits also increases, with the decrease in the minimum value of the population density. This dynamical interplay acts so that population extinction due to stochastic environmental perturbations becomes more likely. This is known as the paradox of enrichment.² However, this does not need to be the only scenario. As discussed by Kuwamura *et al.*,³ the extinction of populations is not always observed in natural enriched environments. In other words, the destabilization effect induced by eutrophication, namely, the enrichment of the environment with nutrients, is somehow canceled in natural ecosystems. Many studies have attempted to clarify mechanisms for stabilizing the population dynamics in enriched environments; see, e.g., Refs. 3 and 4 and references therein.

The investigation reported in this paper is motivated by a study of Kuwamura and Chiba⁵ who explored a mathematical framework supporting a stabilizing mechanism in an enriched environment. The key idea is to consider the differentiation of the predator into active and dormant states. As indicated by a number of studies, dormancy of populations plays an important role in various biological studies.⁶⁻⁹ According to Gyllström and Hansson,⁷ in comfortable environments, zooplankton produces mainly subitaneous eggs. However, fertilized eggs (resting eggs, dormancy state) may be produced in order to escape periods of harsh environmental conditions. Experiments show¹⁰ that the amplitude of prey-predator cycles of *Daphnia* and its algal prey in microcosms increases when a portion of ephippia-producing females is replaced by asexually reproducing gravid females. This suggests that the dormancy of predators may stabilize the population dynamics of *Daphnia* and its algal prey at high nutrient levels.

Under suitable conditions, Kuwamura and Chiba⁵ found that the dormancy of predators induces mixed-mode

I. INTRODUCTION

The equilibrium of the classical prey-predator ecosystems is known to be destabilized when the carrying capacity, i.e., the environment maximal load, of the prey increases.¹ Typically, under this circumstance, prey-predator models display Hopf bifurcations. The effect of such bifurcations is

Note: A preliminary version of this work was presented at the 6th International Conference on Nonlinear Science and Complexity, São José dos Campos, Brazil.

^{a)}Present address: Instituto Dom Luiz, Faculdade de Ciências, Universidade de Lisboa, 1749-016 Lisbon, Portugal

^{b)}Author to whom correspondence should be addressed: jason.gallas@gmail.com

oscillations and chaos in the population dynamics of their prey-predator model. Using the theory of fast-slow systems, they argued that mixed-mode oscillations and chaos bifurcate from a coexisting equilibrium. These results are of interest because they may help to find experimental conditions supporting chaotic population dynamics in a simple phytoplankton-zooplankton (-resting eggs) community in a microcosm with a short duration.

The present paper corroborates the findings of Kuwamura and Chiba⁵ and reports the discovery of a number of novel and intricate behaviors supported by the model. As shown in Fig. 1 (discussed below), we observe remarkably abundant nonchaos-mediated cascades of mixed-mode oscillations in the prey-predator model with dormancy. Mixed-mode oscillations exist in two distinct flavors with signatures which make them easy to distinguish:¹¹ Nonchaos-mediated mixed-mode oscillations display spike-adding sequences, while the more familiar chaos-mediated cascades involve spikes-doubling sequences. In contrast to the standard chaos-mediated cascades, the elusive nonchaos-mediated cascades were discovered quite recently and at present are known only for a handful of situations, namely, for an enzyme reaction,^{11,12} for familiar models of oscillators,^{13,14} and for a centrifugal flywheel governor system.¹⁵ Thus, the observation of nonchaos-mediated cascades in the rather different mathematical context of a biological model adds one more example to the list above.

The model considered here shares a sigmoidal function and some similarities with situations known to lead to very rich dynamics.^{16,17} However, it also contains contributions from quite different terms in the equations of motion, something of interest for our ongoing quest to classify complexity phases in continuous-time dynamical systems.^{18,19} Thus, a closer investigation of the model seems warranted and also motivates the present investigation. Before starting, recall that so far there are no theoretical methods for locating

stability phases corresponding to motions of arbitrary periodicity, going beyond time-honored fixed-point analysis. Therefore, the investigation of complicated oscillatory modes is necessarily of a numerical nature, something feasible nowadays, thanks to the availability of clusters of fast processors and large memories.

II. PREY-PREDATOR MODEL WITH PREDATOR DORMANCY

The model of dormancy effects in the prey-predator population dynamics studied here is defined by a set of three coupled ordinary differential equations^{3,5}

$$\frac{dp}{dt} = r \left(1 - \frac{p}{k} \right) p - f(p)z, \tag{1}$$

$$\frac{dz}{dt} = k_1 \mu(p) f(p)z + \alpha w - d_1 z, \tag{2}$$

$$\frac{dw}{dt} = \epsilon [k_2 (1 - \mu(p)) f(p)z - \alpha w - d_2 w]. \tag{3}$$

Here, p and z denote population densities of prey and predators, respectively, and w is the population density of predators with a dormancy state (resting eggs). Parameters r and k correspond to the intrinsic growth rate and to the carrying capacity of prey, respectively. The function $f(p)$ represents a positive strictly monotone increasing bounded function, taken to be a Holling type II functional response, namely,

$$f(p) = bp / (c + p), \tag{4}$$

where b and c represent the maximum foraging rate and the half saturation constant, respectively. Here, ϵ is a small time-scale separation parameter used to control the speed in the system,⁵ while parameters $k_1 = e/m_1$ and $k_2 = e/m_2$ denote the growth rates of predators in the active and dormant

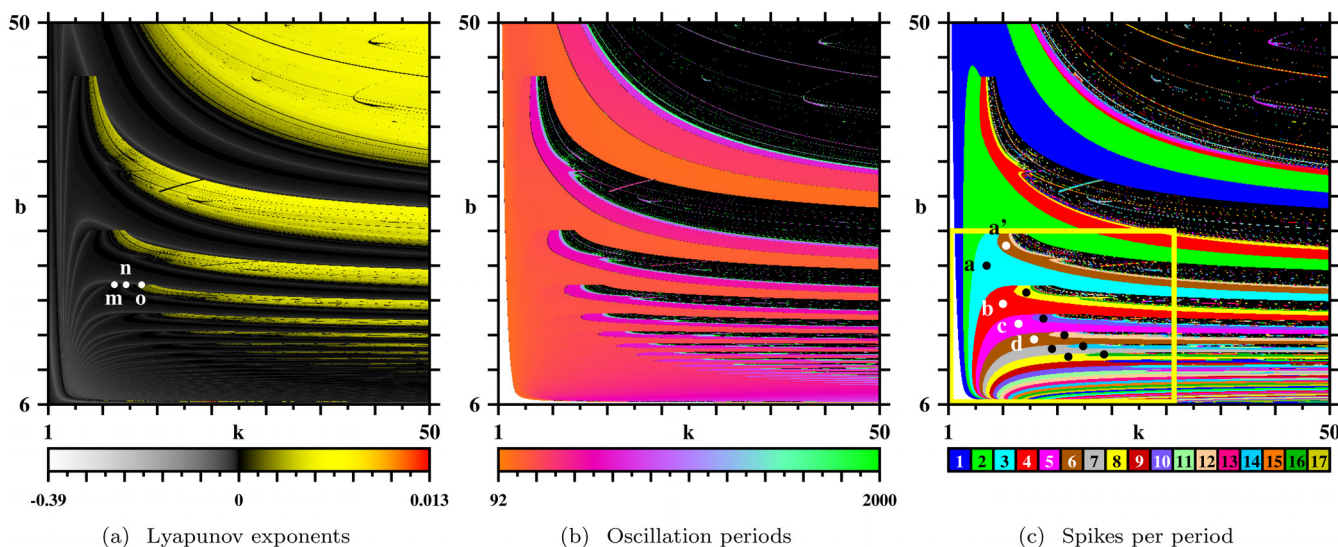


FIG. 1. Three complementary representations of stability: (a) Standard Lyapunov diagram, (b) Diagram displaying the continuous variation of the period, and (c) Isospike diagram, colors indicating the number of spikes per period of periodic oscillations of p . In (b) and (c), non-periodic oscillations (chaos) are represented in black. The information content grows from left to right. Nonchaos-mediated cascades of mixed-mode oscillations are discernible on the leftmost region in (c). The several labels coincide with similar ones shown in Figs. 2, 4, and 5 and are discussed in the text. Each individual panel displays the analysis of a mesh formed by 600×600 equally spaced parameter points. Here $\epsilon = 0.2$.

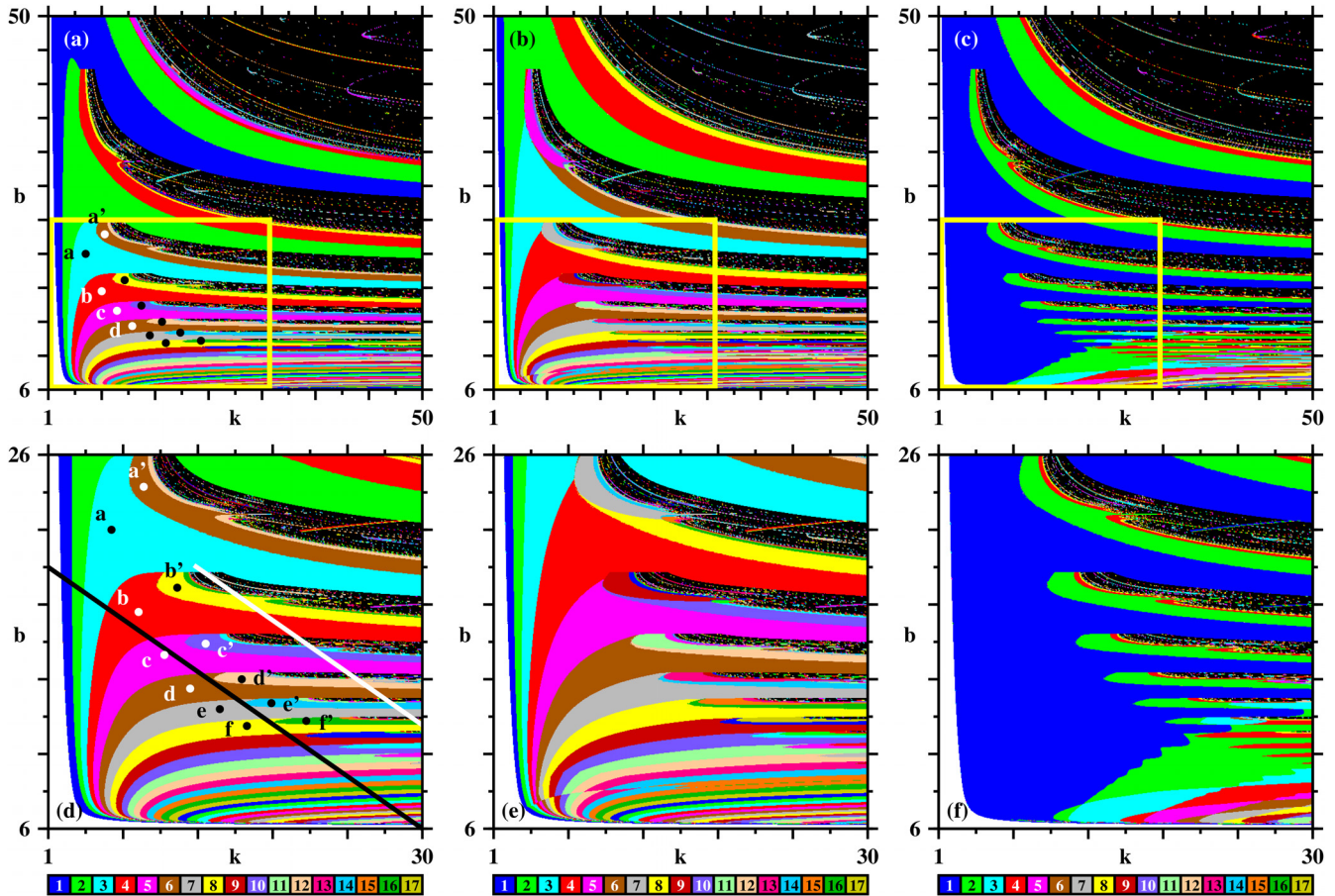


FIG. 2. Nonchaos-mediated cascades of mixed-mode oscillations, illustrated by sequences of domains not separated by chaos (shown in black), as a function of the maximum foraging rate b and the carrying capacity k . Panels (a)–(c) represent the number of domains not separated by chaos as measured for p , z , and w , respectively. The boxes in panels (a)–(c) are shown magnified in panels (d)–(f). The points marked in panels (a) and (d) are the same shown with more detail in Fig. 4, which is a magnification of panel (d). Bifurcations diagrams along the pair of lines in (d) are shown in Fig. 3. Here $\epsilon = 0.2$. Each individual panel displays the analysis of a mesh formed by 600×600 equally spaced parameter points.

states, respectively, that have the following meanings: a predator transforms the food $f(p)$ to reproduction energy with efficiency e , which is distributed to subitaneous and resting eggs with ratios $\mu(p)$ and $1 - \mu(p)$, respectively. As usual, it is given by a sigmoidal function,^{5,16} in the present case by

$$\mu(p) = \frac{1}{2} \left[\tanh\left(\frac{p - \eta}{\sigma}\right) + 1 \right], \quad (5)$$

where η and σ denote the switching level and the sharpness of the switching effect, respectively. This function implies that predators produce more resting eggs than subitaneous eggs when the prey density decreases below a certain level η . Parameters d_1 and d_2 denote the mortality rates of the active and dormant predators, respectively, while α is the hatching rate, i.e., resting eggs have a dormancy period with $1/\alpha$ on average. The model above is an extension of a prey-predator interaction-diffusion system based on the Bazykin model, known as the MacArthur-Rosenzweig model with intraspecific interaction (density-dependent inhibition) among predators, to which the effect of predator dormancy is incorporated. For details, see Ref. 20.

Basically, Kuwamura and Chiba⁵ considered two different situations of the model, $\epsilon = 1$ and $\epsilon = 0.2$, and studied how the bifurcation structure changes as a function k , the

carrying capacity, and with variations of b and d_1 . Unless stated otherwise, the default parameter values used here are the following:⁵

$$r = 0.5, \quad \alpha = 0.02, \quad c = 2, \quad \sigma = 0.1, \quad k_1 = 0.6, \\ b = 2, \quad \eta = 1, \quad d_1 = 0.2, \quad d_2 = 0.0001, \quad k_2 = 0.12.$$

Stability diagrams were constructed by integrating numerically Eqs. (1)–(3) using a standard fourth-order Runge-Kutta method with fixed time-step $h = 0.01$. Integrations were performed horizontally, from left to right, starting from an arbitrary chosen initial condition, $(p, z, w) = (0.6, 0.15, 1.5)$, and proceeding by “following the attractor,”¹⁷ namely, by using the values stored in the computer buffers as initial conditions when incrementing parameters infinitesimally. The first 0.6×10^6 integration steps were disregarded as a transient time needed to come close to the attractor, with an additional of 12×10^6 steps used to compute the Lyapunov spectrum. To find the number of peaks per period, subsequently to the computation of Lyapunov exponents, integrations were continued for 12×10^6 additional time-steps, recording up to 800 extrema (maxima and minima) of the three variables and, from the recorded extrema, determining whether pulses repeated or not, and the number of spikes per period.

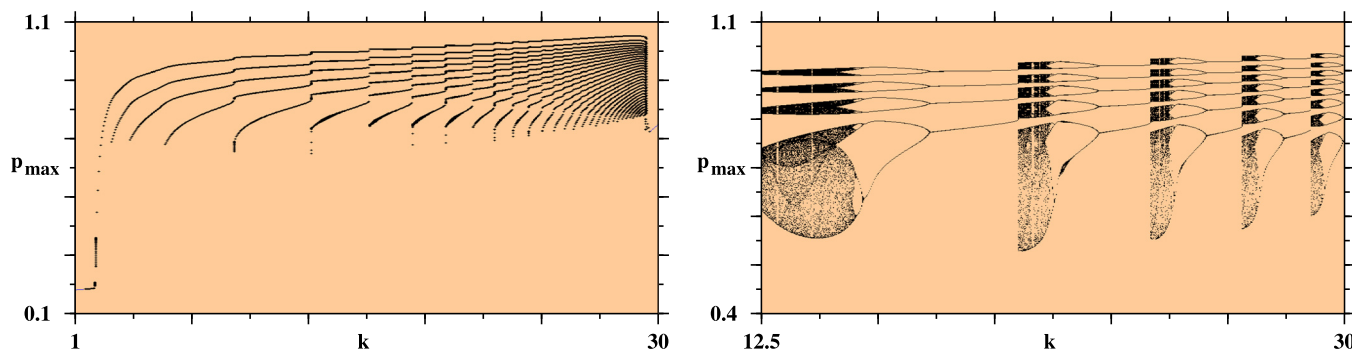


FIG. 3. Plots of p_{\max} , the local maxima of p , contrasting the rather distinct bifurcation diagrams underlying (a) nonchaos-mediated mixed-mode oscillations, and (b) the familiar chaos-mediated cascade. Panel (a) was recorded along the black line in Fig. 2(d), while (b) was recorded along the white line in the same figure. Nonchaos-mediated cascades display spike-adding sequences, while chaos-mediated cascades show spike-doubling.

III. RESULTS

The model described by Eqs. (1)–(3) contains twelve tunable parameters. This means that 66 distinct two-dimensional diagrams are required to represent all possible parameter combinations into stability diagrams. Below, we report a subset containing 29 of these diagrams, covering a considerable portion of the control parameter space. The generation of large sets of stability diagrams involves extensive computations. As far as we know, the present paper reports the largest number of stability diagrams describing complex oscillatory and chaotic phases for a dynamical system. Our stability diagrams are centered around and greatly expand the results obtained previously by Kuwamura and Chiba.⁵ As remarked by them, the chosen parameter values are not inconsistent with experimental results and can be considered as a reference to study the qualitative properties of the population dynamics of phytoplankton-zooplankton communities under the model in Eqs. (1)–(3), although they do not correspond to one identical species.

A. Stability diagrams

Figure 1 illustrates the three complementary stability diagrams obtained. From left to right, the diagrams display the familiar Lyapunov exponents, the period of the oscillations, and the number of spikes contained in each period. This latter diagram, called *isospike diagrams*, uses a palette of 17 colors as indicated by the colorbars to display the number of spikes per period of the stable oscillations. Patterns with more than 17 peaks are plotted by recycling the 17 basic colors modulo 17. Black represents “chaos” (i.e., lack of numerically detectable periodicity), while white and orange

denote non-zero and zero amplitude fixed-points (non-oscillatory solutions), respectively. These conventions are valid for all other stability diagrams reported in this paper. All three panels composing Fig. 1 provide similar dichotomic separation of parameter values leading to periodic oscillations and to chaos. But the information content of the three diagrams increases from left to right, with the isospike diagrams having the greatest information content.

In Fig. 1(b), periods greater than 2000 were represented using the rightmost color in the colorbar. This threshold for the period is necessary in order to avoid obtaining structureless diagrams, since the maximum periods are of the order of 30 000 and do not produce nice diagrams if not limited. For reference, we mention that from the 360 000 points in Fig. 1(b), some 4000 points have periods larger than the threshold 2000 used in the figure. This corresponds to about 1% of the total number of points computed, and about 2% of the parameter points leading to periodic solutions. Below, we use isospike diagrams to characterize the stable oscillations in several sections of the control parameter space.

B. Nonchaos-mediated cascades of mixed-mode oscillations

Figure 2 shows with greater detail typical stability diagrams of the prey-predator system with dormancy [Eqs. (1)–(3)]. The three diagrams in the top row in Fig. 2 display from left to right the number of spikes as observed by following the temporal evolution of the three variables, p , z , and w , respectively. The bottom row shows magnifications of the regions inside the yellow boxes seen on the top panels.

Figure 2 shows a number of interesting facts. The three panels show the precise location where the number of spikes changes for every variable. Oscillations in p and z display a much larger variation of their number of spikes than the oscillations of w which display one spike over extended intervals when b increases. The vertical white stripes seen on the left of the panels show that, independently of b , the maximum foraging rate, the fixed-point is not affected by the carrying capacity k . There is a dynamical threshold for the effects of k to start to be noticed in the system. Furthermore, the onset of chaotic oscillations occurs only for specific ranges of b and k . In particular, the onset occurs for considerably larger values of k when b decreases.

TABLE I. Coordinates (k , b), oscillation period, and number of peaks per period for the twelve p oscillations shown in Fig. 4.

	k	b	Period	Peaks		k	b	Period	Peaks
a	5.9	22.0	253.02	3	a'	8.4	24.3	555.07	6
b	8	17.6	264.54	4	b'	11	18.9	570.85	8
c	10	15.3	280.71	5	c'	13.2	15.9	592.3	10
d	12	13.5	294.14	6	d'	15.9	14.0	619.96	12
e	14.3	12.4	311.59	7	e'	18.3	12.72	649.71	14
f	16.4	11.5	327.54	8	f'	21	11.77	681.35	16

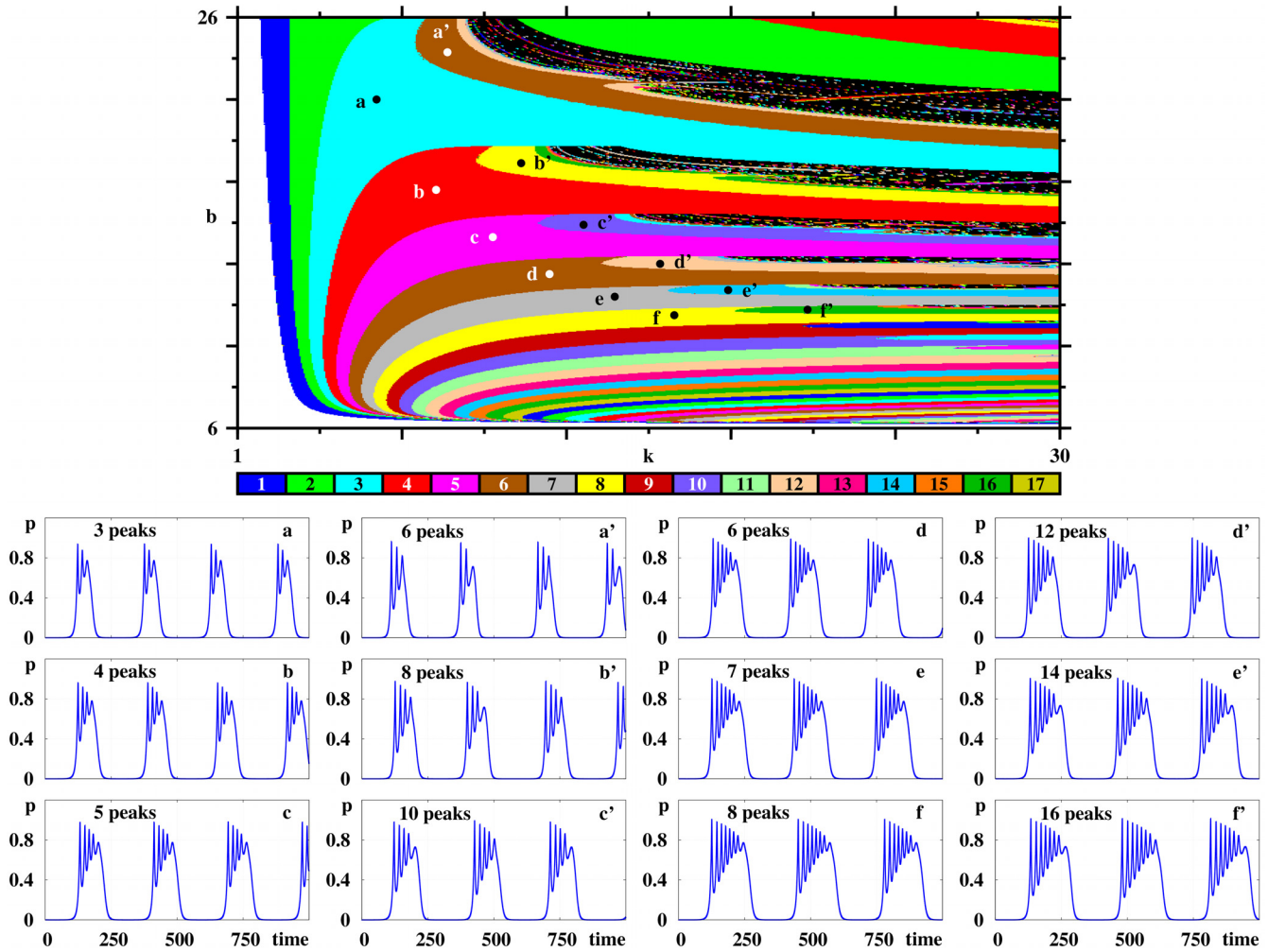


FIG. 4. Typical p -waveforms along the nonchaos-mediated mixed-mode oscillation sequences indicated by the dots. Both sequences show cascades of spike additions and spike doublings. Note the conspicuous presence of a large domain of chaos-free oscillations.¹³ Here, $\epsilon = 0.2$. Evolutions start from the arbitrary initial condition $(p, z, w) = (0.6, 0.15, 1.5)$. Scales on the bottom row apply to all similar panels.

Figure 3 shows a comparison between two cascades of mixed-mode oscillations found in Eqs. (1)–(3), and recorded along the parallel lines seen in Fig. 2(d) and defined by the equations

$$b = -0.483k + 20.483 \quad \text{and} \quad b = -0.483k + 26.035. \quad (6)$$

The diagrams were obtained by starting from $(p, z, w) = (0.6, 0.15, 1.5)$ at the lowest value of k and proceeding by following the attractor until the highest k value. Figure 3(a) illustrates the new cascade of nonchaos-mediated mixed mode oscillations reported in this paper, while Fig. 3(b) shows an example of the chaos-mediated cascade found by Kuwamura and Chiba.⁵ Both cascades look very different and reflect the distinct self-organization of oscillations seen in Fig. 2. Both cascades exist over a relatively wide range of control parameters and, over limited intervals, may be even observed while varying just a single parameter, b , while keeping k fixed.

Comparing Figs. 2(d) and 3(b), it is possible to recognize the existence of multistability: For instance, the smallest values of k along the white line seen in Fig. 2(d) show the existence of period-3 solutions, while the leftmost end of Fig. 3(b) displays chaos and no trace of period-3. Recall that,

when computing stability diagrams by “following the attractor,”¹⁷ the initial conditions are pre-defined only at the start of the computations. When parameters are incremented, one then proceeds by “recycling” the conditions stored in the computer buffer, reached at the end of a previous scan of parameters. Thus, stability diagrams keep record of the exact path followed for their determination and, in particular, may show slight differences as the aforementioned ones.

From Fig. 2(d), it is possible to recognize that the number of spikes increases by one as k grows along the black line. So, a natural question to ask is what exactly happens to the waveforms as they get more and more spikes continuously added to them. Figure 4 provides an answer. On the top panel of this figure, one sees two sequences of points. The leftmost sequence, labeled by unprimed letters, corresponds to stability regions characterized by “primitive” number of spikes, while points on the rightmost sequence, labeled with primed letters, lie inside domains where the number of spikes, and not the period, has doubled. The corresponding waveforms for every point in both sequences are shown under the stability diagram, while their coordinates, period, and number of spikes of their waveforms are collected in Table I. In this table, note that although the number

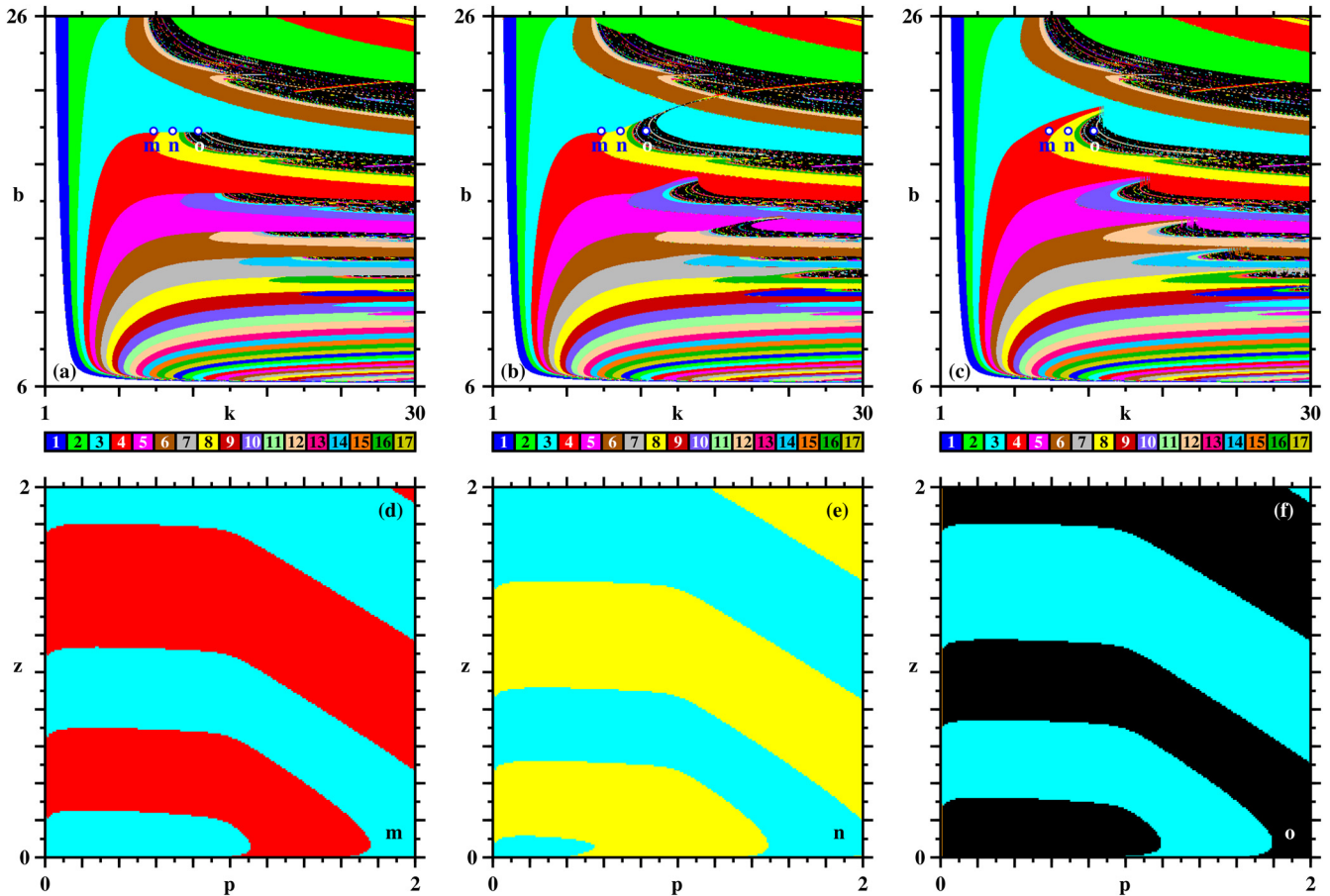


FIG. 5. Multistability in cascades of mixed-mode oscillations. Top row: stability diagrams obtained by: (a) following the attractor from left to right; (b) starting all integrations from a fix initial condition $(p, z, w) = (0.6, 0.15, 1.5)$; (c) Following the attractor from bottom to top. Bottom panels (d)–(f): Basins of attraction for $w = 1.5$ corroborating multi-stability in the blue-white points marked in panel (a)–(c) with coordinates $m = (9.5, 19.8)$, $n = (11, 19.8)$ and $o = (13, 19.8)$. Parameter resolution of individual panels: (a)–(c) 600×600 , (d)–(f) 200×200 parameter points. All panels refer to spikes of p .

of spikes doubles, the corresponding periods vary continuously, being not necessarily doubled. This lack of “period doubling” is a generic characteristic of continuous-time dynamical systems because the period varies continuously with parameters.

A conspicuous feature of Fig. 4 is the presence of a large region of oscillations whose wave patterns evolve continuously but which do not display chaotic oscillations. In fact, in this figure, parameters leading to chaotic oscillations are by far less abundant than the ones leading to stable periodic oscillations. Wide domains of chaos-free oscillations were recently observed in the low-frequency limit of driven oscillators.¹³ But here we find the same phenomena to occur for an autonomous system, i.e., in the absence of any external drive acting on the system. Similar wide chaos-free regions may be also seen in many stability diagrams reported below.

Figure 5 presents the result of an experiment designed to illustrate (i) the presence of multistability as observed in Figs. 2(d) and 3(b), i.e., coexistence of more than one stable oscillation for a given set of control parameters,¹⁰ and (ii) the shape, size, and structure of the boundaries of the basins of attraction for the oscillations supported by the prey-predator model. The panels in the top row of Fig. 5 are similar to the ones in Fig. 2(d) but were obtained by changing the

way of scanning parameters, as described in the caption of the figure. Although changes are relatively small, they can be significant in specific regions. Thin prolongations of stability phases exist abundantly in the diagrams, but larger effects are noticeable in specific regions where chaotic oscillations appear, namely, in the regions similar to the ones containing the labels m , n , and o . The panels in the bottom row of Fig. 5 show that slight parameter changes can induce changes over quite significant regions of phase space. The basin boundaries are not fractal and the relative volume of the initial conditions leading to the coexisting attractors is comparatively similar. The basin structure does not seem to be significantly affected by changes of parameters. Of course, these remarks refer to the very restricted parameter region investigated. A general description of the basin structures remains an interesting open problem.

Figure 6 shows a remarkably complex “braided” self-organization of mixed-mode oscillations discovered for higher values of the carrying capacity k in the $k \times b$ and $k \times d_2$ control planes. In this region of both control parameter space cuts, one finds that the relatively regular sequences of nonchaos-mediated mixed-mode oscillations (seen in upper and lower portions of the panels shown in Fig. 6) are interrupted by a pair of stripes of chaos, represented in black in the diagrams. Between the stripes of chaos, we find

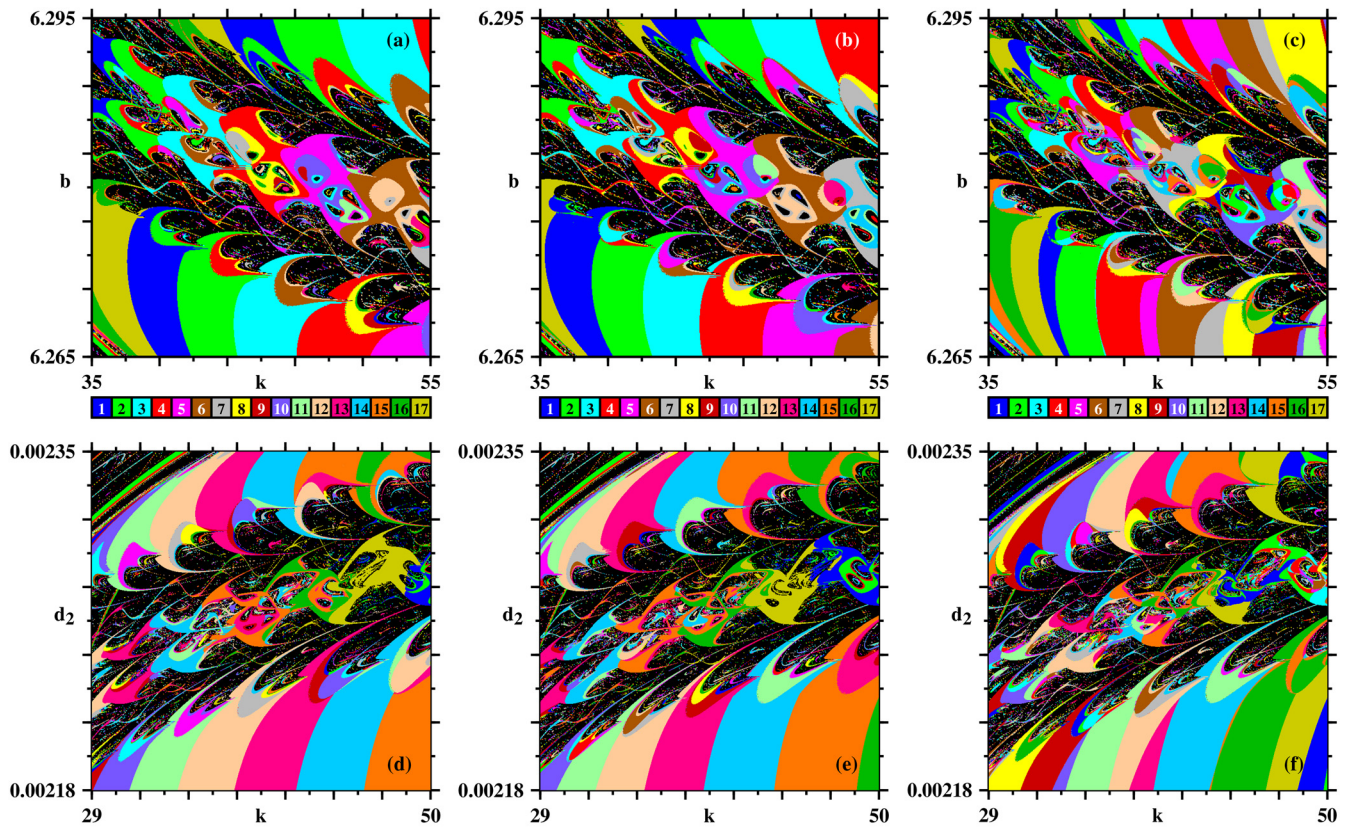


FIG. 6. The complex braided organization of mixed-mode oscillations, embedded between two stripes of chaos (in black), observed at higher values of the carrying capacity k for two cuts: $k \times b$ and $k \times d_2$. Panels on the left, middle, and right columns were obtained by counting spikes per period of p , z , and w , respectively. Details of the oscillations in panels (a) are given in Fig. 7 and Table II. Here, $\epsilon = 0.2$.

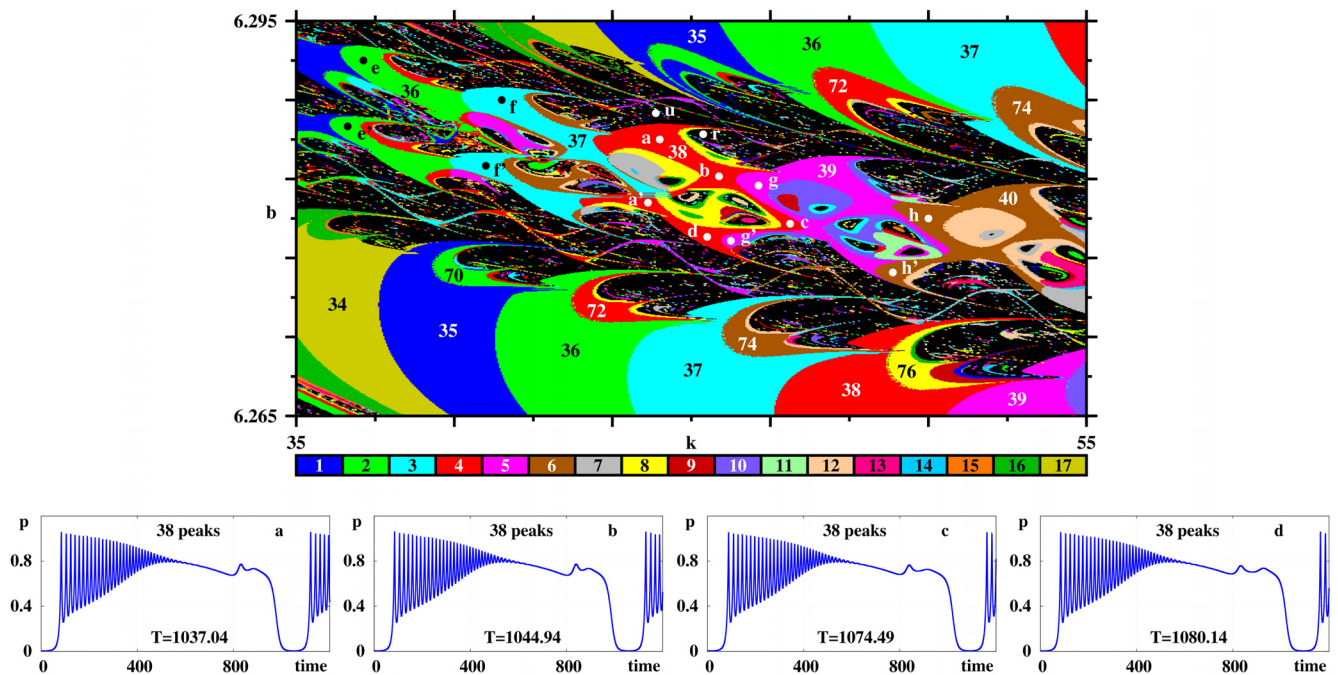


FIG. 7. Top panel: Magnification of Fig. 6(a) illustrating details of the rather complex braided organization found at higher values of the carrying capacity. Numbers indicate the number of spikes per period of the self-similar phases. The four bottom panels show how the waveform and period T of p pulses change when moving clockwise from points $a \rightarrow b \rightarrow c \rightarrow d$, defined in Table II. Here, $\epsilon = 0.2$. Evolutions start from the arbitrary point $(p, z, w) = (0.6, 0.15, 1.5)$. Points u and r mark the parameters whose attractors are shown in Figs. 8(b) and 8(c).

TABLE II. Coordinates (k, b) , period T , and number of spikes per period of p oscillations labeled inside the braided phases in Fig. 7. Here, $\epsilon = 0.2$.

	k	b	Period	Peaks		k	b	Period	Peaks		k	b	Period	Peaks
a	44.2	6.286	1037.04	38						a'	43.9	6.2812	1073.46	38
b	45.7	6.2832	1044.94	38	e	36.7	6.292	994.9	36	e'	36.3	6.287	1034.88	36
c	47.5	6.2796	1074.49	38	f	40.2	6.289	1014.93	37	f'	39.8	6.284	1053.5	37
d	45.4	6.2786	1080.14	38	g	46.7	6.2825	1050.96	39	g'	46	6.2783	1083.58	39
					h	51	6.28	1070.72	40	h'	50.1	6.2759	1101.41	40

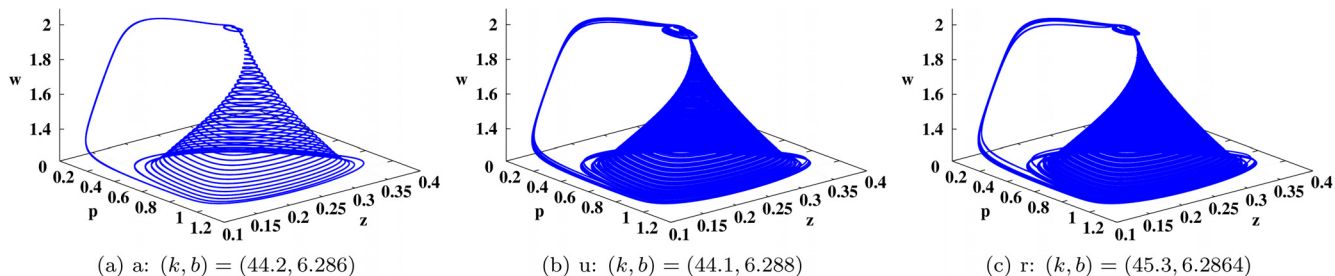


FIG. 8. (a) The “witch hat” surface corresponding to the attractor labeled a in Fig. 7, with 38 spikes per period. All attractors in Fig. 7 produce similar hats. (b), (c) Chaotic witch hats for parameter values close to those in (a), located at points labeled u and r in the top panel in Fig. 7. In all cases, note that the spiraling takes place in the space, not in a plane as it typically happens in Shilnikov’s homoclinic scenario.

a braided sequence of domains arising from oscillations with a relatively high number of spikes per period. The complexity of the stability diagrams in Fig. 6 is best illustrated graphically than described with words.

The organization of oscillations between the stripes of chaos in Fig. 6(a) is magnified and illustrated in more detail in Fig. 7. In this figure, the phase diagram in the top row contains points labeled by letters. It also contains numbers inside

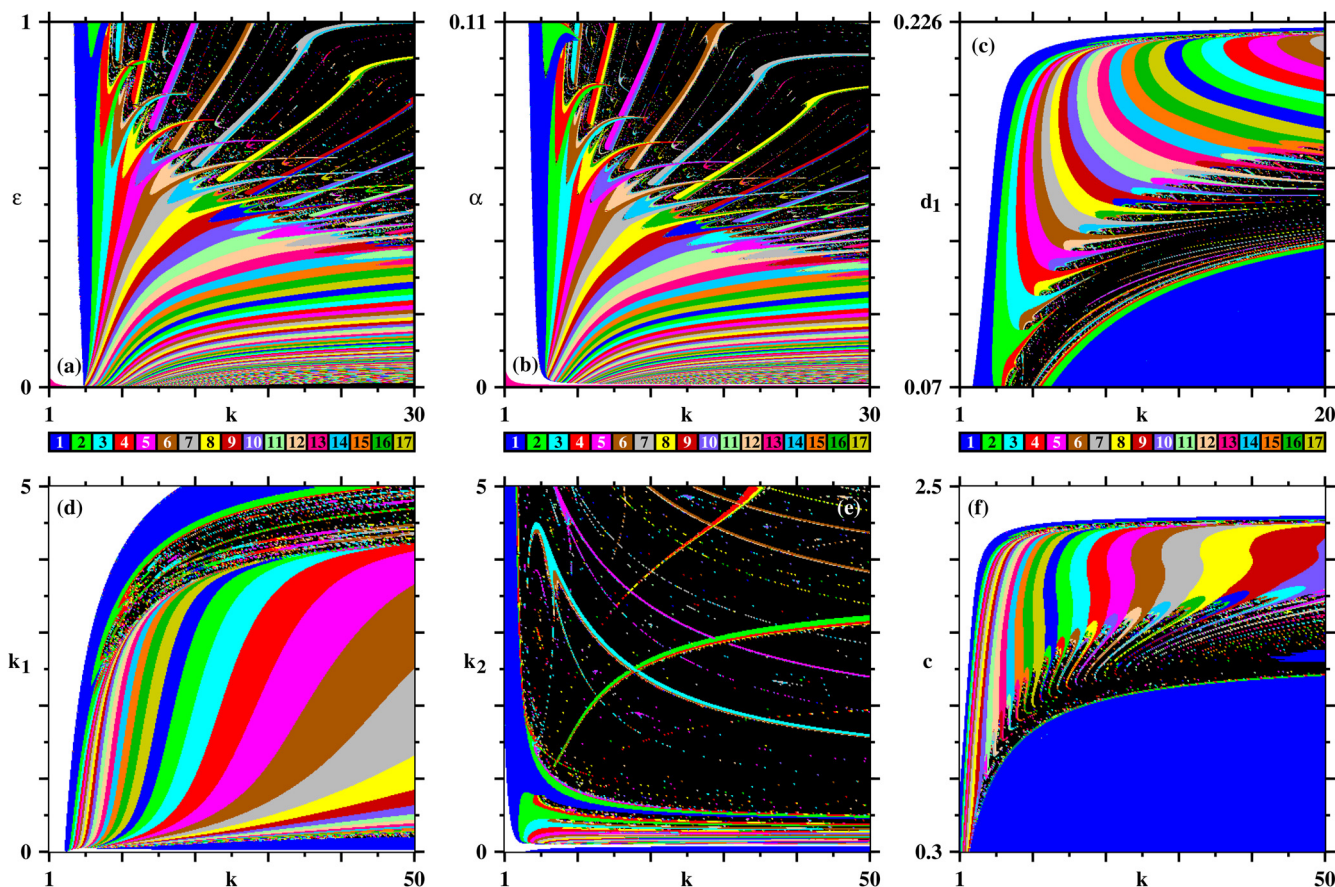


FIG. 9. Wide mosaics illustrating that nonchaos-mediated and chaos-mediated mixed-mode oscillations are also abundant in six additional control parameter planes, obtained by counting spikes per period of p . Here, $b = 7$. Each panel displays the analysis of 600×600 parameter points. Under magnification, panel (e) contains hubs and spirals as described elsewhere.²⁵

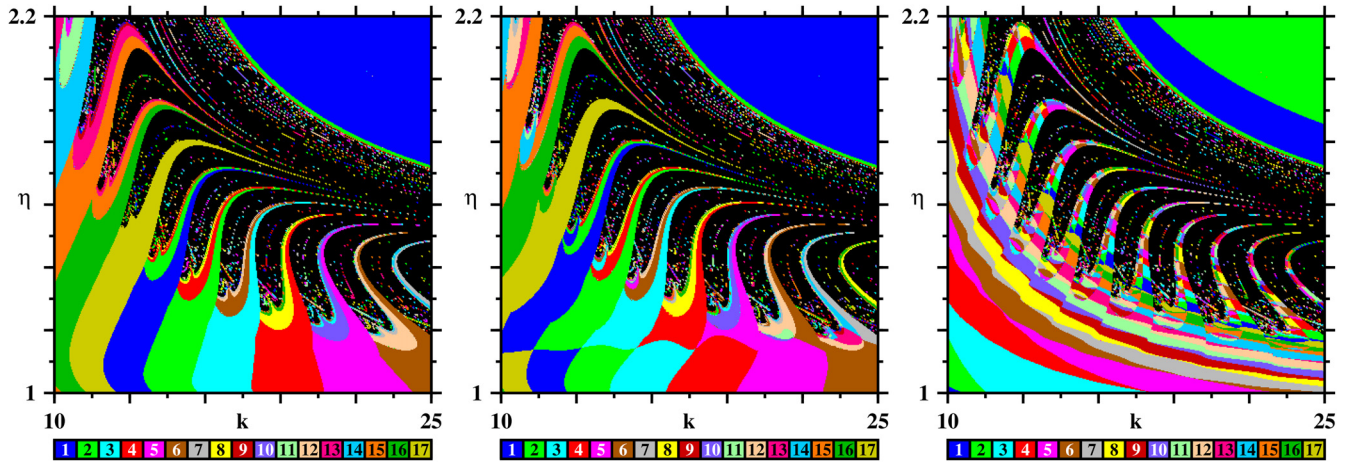


FIG. 10. Stability phases in the $k \times \eta$ plane classified according to the number of peaks of the periodic oscillations in p , z , and w , from left to right, respectively. While the two leftmost panels display relatively similar phases, the rightmost panel shows a rather intricate mosaic of phases. Note the conspicuous horizontal “shear” along $\eta \simeq 1.12$ at the bottom of the center panel. The mechanism underlying the complicated changes in the number of peaks in these and in the next figures is not known. Here, $b = 7$.

the upper and lower cascades of stability islands. Such numbers correspond to the number of spikes of the oscillations characteristic of each island. At about the center of the phase diagram, one sees four points labeled a , b , c , and d , all of them lying inside the same oscillatory phase. As shown in the four panels in the bottom row of Fig. 7, such points are all characterized by trains of periodic oscillations containing 38 spikes per period and, because $38 \bmod 17 = 4$, are represented with the color corresponding to 4 in the colorbar. From the four panels in Fig. 7, it is also possible to see that the period T of the oscillations increases clockwise, from point a to point d , inside the stability islands. The coordinates and characteristics for all points considered in Fig. 7 are given in Table II.

Figure 7 shows the time-evolution of the p variable. The other two variables show similar characteristics and, therefore, were not presented. The information recorded in Table II allows the time-evolution of the waveforms for all three variables to be easily recovered, if needed. An interesting point, however, is to clarify the nature of the reinjection loop responsible for starting every train of pulses shown in Fig. 7. As it is known, an important class of reinjection loops is associated with homoclinic bifurcations of a saddle-focus equilibrium state. In this case, the oscillatory part of the time-evolution corresponds to spiralling occurring essentially on a plane, with the reinjection happening perpendicular to it (see, e.g., Fig. 4 of Ref. 21). Here, however, the spiralling occurs not on a plane but along a conical surface, as illustrated in Fig. 8. As seen from the figure, the spiralling occurs for both periodic and for chaotic orbits. A close inspection of Fig. 8(a) reveals that the pair of spikes which appears between the pulse trains visible in Fig. 7 are responsible for a small loop that exists on the top of the cone in Fig. 8. We conjecture that for other operation regimes of the model, it should be possible to observe more complicated configurations in this region. We have not attempted to locate them since this requires investing considerable additional computer time.

So far, we discussed the properties of nonchaos-mediated mixed-mode oscillations observed on the $k \times b$ and $k \times d_2$

control plane of the model. Is it possible to observe such oscillations in other control planes? Figure 9 shows that it is not only possible to find them in other control planes but, in addition, that they exist over relatively wider parameter windows. Figures 9(a) and 9(b) display a relatively similar structure in the range $1 \leq k \leq 30$, despite the fact that the ranges of ε and α are not the same. Figures 9(c), 9(d), and 9(f) seem to have similar topologies: A common feature is that their upper left corner is white (non-zero amplitude fixed points), meaning that complicated oscillations arise there after Hopf bifurcations. Figure 9(e) displays an apparently distinct structure. However, a magnification of the interval $0 \leq k_2 \leq 1$ reveals a structure resembling the one in Fig. 4. Noteworthy in all these figures is the presence of extended regions where chaos (represented in black) is totally absent. Wide regions of chaos-free oscillations were recently reported for a driven oscillator. Here, however, such chaos-free zones are observed for an undriven, i.e., autonomous, oscillator.

C. Impact of dormancy

The predator dormancy is controlled by the sigmoidal switching function $\mu(p)$, defined in Eq. (5). Such a function contains two parameters, η and σ , representing the switching level and the sharpness of the switching effect, respectively. Figure 10 gives a first idea of the complexity arising when tuning η and k , the carrying capacity. Its three panels record the distribution of the number of spikes per period as a function of the three variables of the model, namely p , z , and w , as indicated in the figure caption. Figures 10(a) and 10(b) show the systematic unfolding of oscillations undergoing progressions of peak additions.¹² In contrast, Fig. 10(c) shows that counting spikes in the variable w result in a much more complicated mosaic of stability phases. The mechanism underlying these complex subdivisions of the control parameter space remains to be determined.

To assess the impact of η and σ on the dynamics, we investigated several additional two-parameter cuts centered

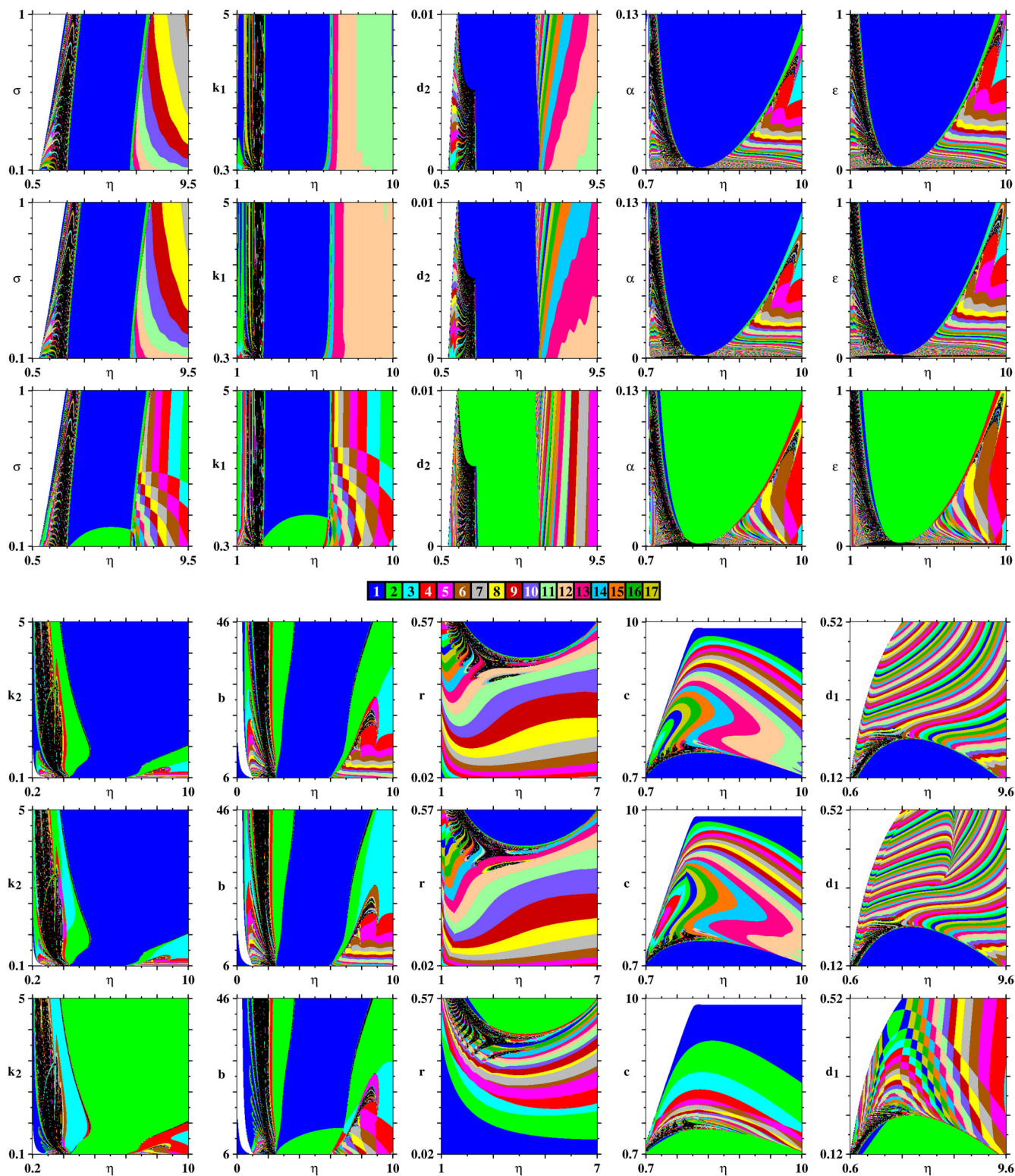


FIG. 11. Stability diagrams as a function of η and ten control parameters. The vertical triplets illustrate stability phases obtained by counting peaks of p , z , and w , from top to bottom, respectively. Note the complex organization of the periodic phases and the relative absence of chaos in all diagrams. White denotes non-zero amplitude fixed points (non-oscillating solutions.) Here, $b = 7$ and $k = 15$.

around the values considered originally by Kuwamura and Chiba.⁵ For selected pairs of parameter values, Figs. 11 and 12 present stability diagrams obtained by counting peaks of p , z , and w as in Fig. 10, but arranging the triplet of panels vertically: the top row shows the panels for the p variable, the panels in the second row for z , and the third row for w .

The same organization was used for the triplets of panels in the three rows at the bottom of the figures.

The leftmost triplet of panels in the upper part of Fig. 11 shows the $\eta \times \sigma$ control plane. From them, one recognizes the central blue stripe, corresponding to tame oscillations having a single peak per period, that dominates more than one third of

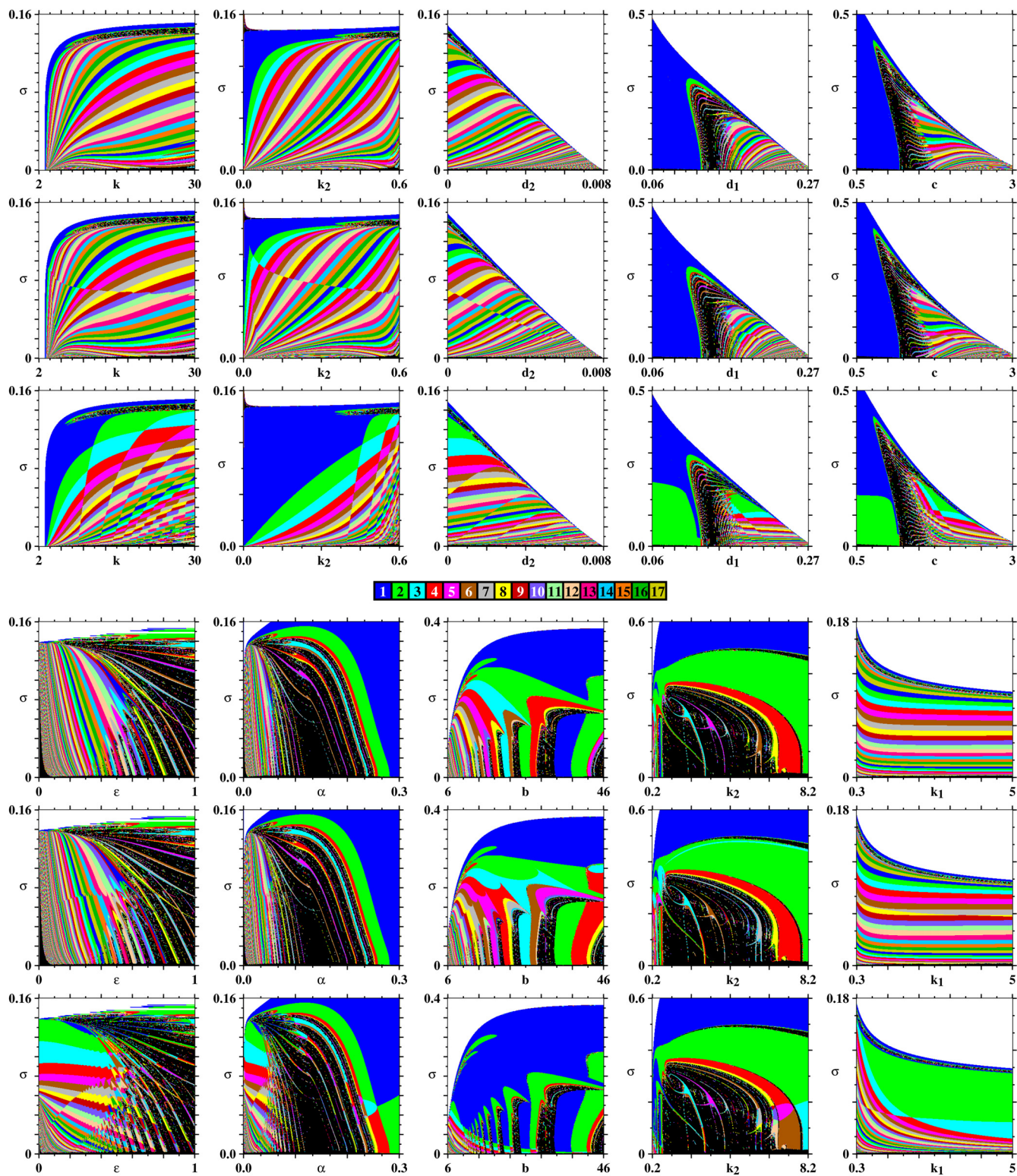


FIG. 12. Stability diagrams as a function of σ and ten control parameters, with vertical triplets illustrating phases obtained by counting peaks of p , z , and w , from top to bottom, respectively. Note the complex organization of the periodic phases. in all diagrams. White denotes non-zero amplitude fixed points (non-oscillating solutions.) Here, $b = 7$ and $k = 15$.

the figure. In contrast, complex oscillatory phases lie on both sides of this central stripe. To the left of the central stripe, one finds a wide phase resulting from chaotic oscillations, while to the right there is no chaos. In Fig. 11, we collected diagrams that resemble somewhat the organization just described.

Clearly, the complicated organization of oscillatory phases makes it hard to find unifying themes covering all panels.

From a dynamical point of view, the predator-prey model of Eqs. (1)–(3) is very appealing because it involve a triplet of equations that scramble the three variables in a

unique way. For instance, consider the generic form of a dissipative oscillator²²

$$\ddot{x} + a\dot{x} = F, \quad \dot{F} = f(x), \quad (7)$$

where x is the independent variable, a is the friction, and $f(x)$ is a nonlinear function of x which may depend on one or more parameters. The above equation may be equivalently written as a flow system of three equations, namely

$$\dot{x} = y, \quad (8)$$

$$\dot{y} = z, \quad (9)$$

$$\dot{z} = -az - y + f(x). \quad (10)$$

For quite a number of $f(x)$, this equation is known for producing mathematically intricate dynamics as reported continuously during more than three decades, e.g., by Glendinning.²³ A very recent result concerning the flow above, involving perhaps the simplest form of a system governed by Eqs. (8)–(10), is the single op-amp-based jerk circuit.²⁴ Comparing Eqs. (8)–(10) with Eqs. (1)–(3), it seems plausible to expect the nonlinearities present in the latter to complicate the resulting stability diagrams. Regrettably, there are yet no theoretical tools allowing one to anticipate features of stability diagrams for sets of differential equations. Fortunately, powerful computer clusters allow one to study systematically the auto-organization of stability.

Figure 12 shows the dependence on σ of several control planes, in the same vein as the η dependence is presented in Fig. 11. The panels were grouped so that “similar” diagrams are displayed close to each other. Generically, the overall message from Figs. 11 and 12 is that changes in η and σ result in rather distinct stability phases. Clearly, it is not easy to summarize the global dynamical effect of changing parameters, because every change of parameters results in significant changes on the stability charts. With hindsight, the aforementioned statement that the chosen parameter values are not inconsistent with experimental results⁵ seems relatively innocuous because a plethora of other choices of parameters values also lead to similarly complex dynamics. In other words, there is no short supply of complicated dynamics supported by the model in Eqs. (1)–(3). The dynamical richness of the model certainly deserves further study.

The plane $k \times k_2$ in Fig. 9(e) as well as planes $\eta \times k_2$ in Fig. 11 and $k_2 \times \sigma$ in Fig. 12 seems to contain a profusion of hubs and spirals similar to the ones first observed in a simple resistive circuit.²⁵ Furthermore, among others, the planes $\alpha \times \sigma$ and $k_2 \times \sigma$ clearly display the *arborescent patterns* first described for a three-cell population model of cancer (see Figs. 6 and 7 in Ref. 26). The detailed exploration of all these rich scenarios demands a considerable additional investment of computer time and will not be attempted here.

IV. CONCLUSIONS

The impact of predator dormancy on the population dynamics of phytoplankton-zooplankton in freshwater ecosystems was investigated using a simple model previously considered by Kuwamura and Chiba.⁵ Predator dormancy

was linked to nonchaos-mediated sequences of oscillations, a novel and elusive type of mixed-mode oscillations. As the carrying capacity increases, nonchaos-mediated sequences were found to emerge well before the onset of chaos in the system, i.e., before the onset of the more familiar chaos-mediated sequences. From a dynamical point of view, the observation of nonchaos-mediated sequences in the system is of interest because such sequences have been reported only recently and, at present time, are known to exist only in a few systems.^{11–15} At present, the few reports of nonchaos-mediated sequences allow no definitive comparison concerning their origin and unfolding. As seen in Fig. 9 when $\epsilon \rightarrow 0$, nonchaos-mediated sequences display intricate accumulation limits, which remain to be investigated, in particular to understand the interplay between the fast and slow time-scales present in the system. In addition, as seen in Figs. 6, 7, and 9, stability phases emerge in control parameter space which are self-organized quite regularly but in a morass of ways, complicated beyond description, which are best represented by graphical means rather than by words.

In the present paper, we considered 29 out of the 66 possible two-dimensional stability sections of the multidimensional control parameter space. We see no reason for nonchaos-mediated cascades of oscillations not to exist also for the parameter combinations that were not investigated here. However, a full exploration of all possible combinations is a task demanding considerable additional computations and must be postponed. Our present computations extend considerable knowledge about the population dynamics of phytoplankton-zooplankton in fresh water ecosystems using a simple model including dormancy. The stability diagrams reported here represent by far the most detailed exploration of the parameter space of a dynamical system depending on many parameters. The discussion of the phenomena recorded in these stability diagrams is necessarily descriptive due to the lack of a mathematical framework to address motions with higher periodicities and chaotic oscillations. While some of the parameter spaces considered are clearly not easy to access experimentally, they nevertheless display a complicated self-organization whose structure is rather novel, particularly since they arise in a system not acted by any external drive. It would be of interest to discover the mechanisms underlying such self-organization. Finally, we mention that it would be also interesting to detect the fine structure of the parameter spaces in ecology in real experiments. A nice long-term experiment reporting evidence of chaos in a plankton community²⁷ provides some hope of the feasibility of such detection in the dynamics of zoo-phytoplankton.

ACKNOWLEDGMENTS

J.G.F. was supported by a postdoctoral fellowship from the FCT, Portugal (SFRH/BPD/101760/2014). JACG was supported by CNPq, Brazil. All phase diagrams were computed on the CESUP-UFRGS Supercomputing Center located in Porto Alegre, Brazil.

¹M. L. Rosenzweig and R. H. MacArthur, “Graphical representation and stability conditions of predator-prey interactions,” *Am. Nat.* **97**, 209–223 (1963).

- ²M. L. Rosenzweig, "Paradox of enrichment: Destabilization of exploitation ecosystems in ecological time," *Science* **171**, 385–387 (1971).
- ³M. Kuwamura, T. Nakazawa, and T. Ogawa, "A minimum model of prey-predator system with dormancy of predators and the paradox of enrichment," *J. Math. Biol.* **58**, 459–479 (2009).
- ⁴C. X. J. Jensen and L. R. Ginzburg, "Paradox or theoretical failures? The jury is still out," *Ecol. Model.* **188**, 3–14 (2005).
- ⁵M. Kuwamura and H. Chiba, "Mixed-mode oscillations and chaos in a prey-predator system with dormancy of predators," *Chaos* **19**, 043121 (2009).
- ⁶V. Alekseev and W. Lampert, "Maternal control of resting-egg production in Daphnia," *Nature* **414**, 899–901 (2001).
- ⁷M. Gyllström and K.-A. Hansson, "Dormancy in freshwater zooplankton: Induction, termination and the importance of benthic-pelagic coupling," *Aquat. Sci.* **66**, 274–295 (2004).
- ⁸N. G. Hairston, Jr., A. M. Hansen, and W. R. Schaffner, "The effect of diapause emergence on the seasonal dynamics of a zooplankton assemblage," *Freshwater Biol.* **45**, 133–145 (2000).
- ⁹C. Ricci, "Dormancy patterns in rotifers," *Hydrobiologia* **446**, 1–11 (2001).
- ¹⁰E. McCauley, R. M. Nisbet, W. W. Murdoch, A. M. de Roos, and W. S. C. Gurney, "Large-amplitude cycles of Daphnia and its algal prey in enriched environments," *Nature* **402**, 653–656 (1999).
- ¹¹M. J. B. Hauser and J. A. C. Gallas, "Nonchaos-mediated mixed-mode oscillations in an enzyme reaction system," *J. Phys. Chem. Lett.* **5**, 4187–4193 (2014).
- ¹²M. R. Gallas and J. A. C. Gallas, "Nested arithmetic progressions of oscillatory phases in Olsen's enzyme reaction model," *Chaos* **25**, 064603 (2015).
- ¹³J. G. Freire, M. R. Gallas, and J. A. C. Gallas, "Chaos-free oscillations," *Europhys. Lett.* **118**, 38003 (2017).
- ¹⁴J. G. Freire, M. R. Gallas, and J. A. C. Gallas, "Stability mosaics in a forced Brusselator: Auto-organization of oscillations in control parameter space," *Eur. Phys. J. Special Topics* **226**, 1987–1995 (2017).
- ¹⁵X. Rao, Y. Chu, Lu-Xu, Y. Chang, and J. Zhang, "Fractal structures in centrifugal flywheel governor system," *Commun. Nonlinear Sci. Numer. Simul.* **50**, 330–339 (2017).
- ¹⁶J. G. Freire, T. Pöschel, and J. A. C. Gallas, "Stern-Brocot trees in spiking and bursting of sigmoidal maps," *Europhys. Lett.* **100**, 48002 (2012).
- ¹⁷J. G. Freire, R. J. Field, and J. A. C. Gallas, "Relative abundance and structure of chaotic behavior: The nonpolynomial Belousov-Zhabotinsky reaction kinetics," *J. Chem. Phys.* **131**, 044105 (2009).
- ¹⁸L. Junges and J. A. C. Gallas, "Intricate routes to chaos in the Mackey-Glass delayed feedback system," *Phys. Lett. A* **376**, 2109–2116 (2012).
- ¹⁹J. A. C. Gallas, "Spiking systematics in some CO₂ laser models," *Adv. At., Mol., Opt. Phys.* **65**, 127–191 (2016).
- ²⁰M. Kuwamura, "Turing instabilities in prey-predator systems with dormancy of predators," *J. Math. Biol.* **71**, 125–149 (2015).
- ²¹R. Vitolo, P. Glendinning, and J. A. C. Gallas, "Global structure of periodicity hubs in Lyapunov phase diagrams of dissipative flows," *Phys. Rev. E* **84**, 016216 (2011).
- ²²A. A. Andronov, A. A. Vitt, and S. E. Khaikin, *Theory of Oscillations* (Dover, New York, 1966), translation of the 1937 Russian original.
- ²³P. Glendinning, "Bifurcations near homoclinic orbits with symmetry," *Phys. Lett. A* **103**, 163–166 (1984).
- ²⁴R. Tchitnga, T. Nguazon, P. H. L. Fotso, and J. A. C. Gallas, *IEEE Trans. Circuit Syst. II* **63**, 239–243 (2016).
- ²⁵C. Bonatto and J. A. C. Gallas, "Periodicity hub and nested spirals in the phase diagram of a simple resistive circuit," *Phys. Rev. Lett.* **101**, 054101 (2008).
- ²⁶M. R. Gallas, M. R. Gallas, and J. A. C. Gallas, "Distribution of chaos and periodic spikes in a three-cell population model of cancer: Auto-organization of oscillatory phases in parameter space," *Eur. Phys. J. Special Topics* **223**, 2131–2144 (2014).
- ²⁷E. Benincà, J. Huisman, R. Heerkloss, K. D. Jöhnk, P. Branco, E. H. Van Nes, M. Scheffer, and S. P. Ellner, "Chaos in a long-term experiment with a plankton community," *Nature* **451**, 822–826 (2008).